Ocean acidification enhances primary productivity and nocturnal carbonate dissolution in intertidal rock pools

Narimane Dorey, Sophie Martin, Lester Kwiatkowski

Biogeosciences

Research article

Ocean acidification enhances primary productivity and nocturnal carbonate dissolution in intertidal rock pools

Narimane Dorey[1], **Sophie Martin**[2], **and Lester Kwiatkowski**[3]

[1]LMD-IPSL, CNRS, École Normale Supérieure/PSL Res. Univ., École Polytechnique,
Sorbonne Université, 75005 Paris, France
[2]CNRS, Sorbonne Université, Laboratoire Adaptation et Diversité en Milieu Marin, UMR 7144,
Station Biologique de Roscoff, Place Georges Teissier, 29680 Roscoff, France
[3]LOCEAN Laboratory, Sorbonne Université-CNRS-IRD-MNHN, 75005 Paris, France

Correspondence: Narimane Dorey (narimane.dorey@gmail.com)

Abstract. Human CO_2 emissions are modifying ocean carbonate chemistry, causing ocean acidification and likely already impacting marine ecosystems. In particular, there is concern that coastal, benthic calcifying organisms will be negatively affected by ocean acidification, a hypothesis largely supported by laboratory studies. The interrelationships between carbonate chemistry and marine calcifying communities in situ are complex, and natural mesocosms such as tidal pools can provide useful community-level insights. In this study, we manipulated the carbonate chemistry of intertidal pools to investigate the influence of future ocean acidification on net community production (NCP) and calcification (NCC) at emersion. Adding CO_2 at the start of the tidal emersion to simulate future acidification ($+1500 \, \mu atm \, pCO_2$, target pH 7.5) modified net production and calcification rates in the pools. By day, pools were fertilized by the increased CO_2 ($+20\%$ increase in NCP, from 10 to $12 \, mmol \, O_2 \, m^{-2} \, h^{-1}$), while there was no measurable impact on NCC. During the night, pools experienced net community dissolution (NCC < 0), even under present-day conditions, when waters were supersaturated with regard to aragonite. Adding CO_2 to the pools increased nocturnal dissolution rates by 40% (from -0.7 to $-1.0 \, mmol \, CaCO_3 \, m^{-2} \, h^{-1}$) with no consistent impact on nocturnal community respiration. Our results suggest that ocean acidification is likely to alter temperate intertidal community metabolism on sub-daily timescales, enhancing both diurnal community production and nocturnal calcium carbonate dissolution.

1 Introduction

The ongoing increase in anthropogenic carbon dioxide (CO_2) in the atmosphere and the ocean – resulting in ocean acidification – is likely to create adverse living conditions for marine coastal communities (IPCC, 2019). Ocean acidification is projected to further decrease average surface pH by up to 0.4 units by 2100 (SSP5-8.5 scenario; Kwiatkowski et al., 2020) and is identified as a major threat to marine ecosystems (IPCC, 2019). Lower seawater pH has significant effects on marine organisms' physiology and fitness, from altered survival and reduced growth (see review by Kroeker et al., 2013) to changes in pH homeostasis (e.g., Kottmeier et al., 2022) and metabolic rates, energy trade-offs (e.g., Dorey et al., 2013; Pan et al., 2015), and reduced feeding efficiency (e.g., Stumpp et al., 2013). Marine calcifiers – the builders of calcified structures ($CaCO_3$) – have been a focus of ocean acidification research due to the sensitivity of calcification to the carbonate saturation state (Ω), defined as follows:

$$\Omega = [Ca^{2+}][CO_3^{2-}]/K'_{sp},$$

where K'_{sp} is the stoichiometric solubility product for the considered carbonate polymorph (i.e., Ω_a for aragonite or Ω_c for calcite). The saturation state depends on temperature, pH and pressure (lower Ω when pH or temperature decreases, and pressure increases). When $\Omega < 1$, inert carbonate minerals tend to dissolve. The polymorphs composing the calcified structure like calcite and to a greater extent aragonite and high-magnesium calcite are prone to dissolution when pH

decreases. For instance, in Atlantic surface waters (at $20\,°C$), saturation state equilibrium ($\Omega = 1$) is reached at pH 7.3 ($pCO_2 = 2650\,\mu atm$) for calcite but at pH 7.6 ($1250\,\mu atm$) for aragonite. For high-magnesium calcite, experiments from Yamamoto et al. (2012) demonstrate that inert (dead) high-magnesium calcite from coralline algae passively dissolves at Ω_a values between 3.0 and 3.2 (see also Ries et al., 2016). Organisms with calcified structures are thus likely to experience reduced net calcification due to ocean acidification through both enhanced dissolution and reduced gross calcification rates.

Aside from acidifying the ocean (increased H^+), increased ocean CO_2 uptake could affect the productivity of algae and marine plants. As CO_2 dissolves in the ocean, the dissolved inorganic carbon (DIC; CO_2, HCO_3^- and CO_3^{2-}) concentration increases. DIC is the substrate for marine photosynthesis (mainly CO_2 and HCO_3^-), and as such, it can limit photosynthetic rates when scarce. In algae and marine plants that are carbon-limited (permanently or periodically), elevated DIC could also directly increase photosynthetic rates, and Mackey et al. (2015) propose that these rates could be further increased by the higher concentration gradient between water and the photosynthetic cells. However, the authors point out that while positive effects are theoretically expected, they may be small, specific to species' biology and the environment they live in, and difficult to predict (see also Hurd et al., 2019). In terrestrial ecosystems, the Intergovernmental Panel on Climate Change defines CO_2 fertilization as "the enhancement of plant growth as a result of increased atmospheric CO_2 concentration" (Jia et al., 2019) and reports that CO_2 fertilization has likely already happened, although the magnitude of this effect depends on the plants, assemblages or ecosystems considered (and on other factors constraining growth).

The response of single species to changes such as ocean acidification and increased DIC concentrations is often insufficient to predict community-level impacts. Ecological interactions such as competition or predation can affect the outcome of perturbation experiments (Kroeker et al., 2013). For instance, Paiva et al. (2021) showed that the laboratory growth of an isopod species was an order of magnitude slower than when raised in the presence of other species from its community. In another study, Legrand et al. (2019) showed that the presence of grazers increased coralline algal calcification ($+50\,\%$ in winter and $+100\,\%$ in summer), but when grazers were combined with ocean acidification, algal calcification decreased more than with acidification alone. Not taking into account such interactions can therefore result in poor characterization of the effects of ocean acidification. Furthermore, while critical for a mechanistic understanding of the processes affecting marine biota, laboratory studies are seldom realistic. Typically performed under controlled, simplified and stable conditions (e.g., with respect to temperature and food), laboratory studies can better assess the effect of pH alone (Widdicombe et al., 2010). However, exposure to a stable pH (e.g., 7.6 vs. 8.0) fails to reflect the daily and seasonal variability observed in natural ecosystems, in particular coastal ones (Torres et al., 2021). Natural mesocosm perturbation experiments are thus essential tools to investigate future changes in variable and complex ecosystems, which are difficult to capture in the lab (Barry et al., 2010; Andersson et al., 2015).

Most in situ mesocosm experiments investigating the effect of ocean acidification have been conducted on planktonic communities, kept in large "bags" equilibrated to the desired pH (Riebesell et al., 2013). These studies demonstrate that adding CO_2 can significantly change the organization of the plankton community (Spisla et al., 2021) and increase autotrophic biomass under high-nutrient conditions (Schulz et al., 2013). Due to the technical challenges, however, benthic calcifying communities are seldom manipulated this way in situ (Widdicombe et al., 2010). Two such manipulation experiments are the studies by Albright et al. (2016, 2018), where the authors used NaOH and CO_2 to reproduce pre-industrial and future pH conditions on a coral reef and found evidence that reef growth had been reduced by $7\,\%$ over the industrial era and was likely to decline further. Other studies have investigated such community-level effects by either simulating "artificial", simpler assemblages in laboratory setups (e.g., Cox et al., 2015; Pansch et al., 2016) or using phenomena such as natural CO_2 vents. For instance, in the vents of Ischia, as pH decreases, the presence of calcifying species declines (see review by Foo et al., 2018). Alternatively, Kwiatkowski et al. (2016) used locally induced acidification due to respiration (no CO_2 addition) in tidal pools, a naturally closed system, and demonstrated that nighttime dissolution of these communities was positively correlated with Ω. Here, we used tidal pools of the English Channel as ephemeral mesocosms, where we modified carbonate chemistry conditions at the start of emersion through CO_2 addition.

Temperate rocky tidal pools – or rock pools – are highly dynamic systems that have been long studied by naturalists since they are easy to reach, and their ecosystem structure generally resembles subtidal benthic communities (Ganning, 1971). Tidal pool organisms from the upper shore, well adapted to pool conditions, form typical benthic communities: often low in diversity, they consist of a few characteristic macroalgal (e.g., *Ulva* sp.) and animal species (e.g., limpets). In winter, red macroalgae – including calcifying algae – often dominate the pools, and while they do not disappear in summer, a bloom of soft green macroalgae is generally observed during the warm season. Temperature, salinity, oxygen and pH in the pools are extremely variable, often far outside the seasonal range of nearby free-flowing seawater (Legrand et al., 2018a; Morris and Taylor, 1983). Tidal pools generally emerge from the ocean twice a day in regions of semidiurnal tides, with the duration dependent on shore location and the tidal coefficient. On short timescales tidal pools act as closed systems, with carbonate chemistry easily ma-

nipulated and temporal changes reflecting in situ community metabolism (no water mass transport and negligible air–sea gas exchange).

In the present study, we used tidal pools as natural mesocosms to investigate the effect of ocean acidification on communities dominated by calcifying red algae. We measured diurnal and nocturnal net community calcification and production (or respiration) following CO_2 addition across three seasons (winter, spring and summer) to assess how tidal pool community metabolism may respond to end-of-the-21st-century high ocean acidification (pH 7.5).

2 Material and methods

2.1 Field site

The experiments were performed on a rocky intertidal shore characterized by granitic substrate on the north coast of Brittany, France, between 2019 and 2021. The beach of Bloscon (48°43′30.0″ N, 3°58′10.5″ W) is situated in Roscoff at the entrance of the Bay of Morlaix and has a hydrology principally affected by the waters of the English Channel and to a lesser extent the Penzé and Morlaix rivers (Fig. 1). This area is characterized by strong, oscillating, semidiurnal tides of up to 9 m. Temperatures are generally low in the deeper-flowing water (from 9–10 °C in winter to 16–17 °C in summer), and salinity is close to that of the adjacent Atlantic (~ 35; see Fig. S1 in the Supplement for detailed temperature and salinity data from the two monitoring stations Estacade and Astan; these stations are part of the Service d'Observation en Milieu Littoral, SOMLIT, a network described in Cocquempot et al., 2019).

2.2 Tidal pool characterization

For this study, we chose five tidal pools with high coverage in calcifying algae ($\geq 30\%$ of the pool surface area). Both crustose (CCA) and articulated (branching) coralline algae (ACA) were present. The field site has an eastern exposure, resulting in full morning sun and relatively early shade in the evening. Foreshore locations of the pools resulted in daily emersion year-round including during neap tides (midtide, approx. 5–6 m above chart datum). Pools emerged for 6–7 h during low-tide periods. During that time, pools were completely separated from the adjacent open water, and their depths were effectively constant in winter (low-evaporation season), an indication that there was no seawater leakage.

The volume of each of the five pools (from 16 to 39 L; Fig. 2) was estimated in April 2021, at the end of the emersion period just before high-tide flooding, by measuring salinity changes when a known volume of freshwater was added and well mixed. To estimate the pools' initial volumes, we also took into consideration the measured salinity changes throughout the emersion period to estimate evaporative losses and combined this with the volume directly lost

through water sampling (see below). The pool projected area and the relative area covered by each type of algae were estimated from scaled aerial photographs and analyzed using ImageJ (US National Institutes of Health, Bethesda, Maryland, USA, https://imagej.nih.gov/ij, last access: 1 June 2022). Pool area ranged from 0.3 to 0.7 m^2 (Fig. 2). The pools had slightly different community composition, with dominant calcifying red algae represented by *Lithophyllum incrustans* (CCA: 30 to 77 % of the benthic cover) and *Ellisolandia elongata* (ACA: 0 to 6 % of the benthic cover). The remaining pool area was either free of algal cover with only bare granitic rock visible or covered by soft macroalgae. In summer (September 2020 and 2021), the pools also hosted the green algae *Ulva* sp. and *Enteromorpha* sp. (2 % to 44 % of the benthic cover; see Supplement file SP1-2 for results detailed by season) and, in Pool E, small single branches of the brown algae *Sargassum muticum*, covering less than 0.5 % of the pool. One limit of this method of aerial photography is that it only takes into account what is visible from above (2D). These estimates may thus be biased against algae that were hidden under the green algae canopy in summer or that were in crevices/under rocks. We also noted the presence of diverse heterotrophs such as anemones, sea sponges, small gobies and shrimps. Calcifying invertebrates were represented by four gastropod species: *Phorcus lineatus*, *Patella ulyssiponensis*, *Patella vulgata* and *Gibbula pennanti*.

2.3 Study design and seawater manipulation

Fieldwork was conducted during the low-tide emersion periods during the day and night. We refer to the period from the beginning to the end of the pool emersion as a "low-tide emersion period" and to each seasonal sampling period as a "field session" (Table 1). We sampled during three seasons: winter (February 2020 and 2021), spring (April 2021) and summer (September 2020 and 2021). During each field session, all the pools experienced both "future" (approximately the year 2100 under high emissions) and present-day ("present", non-manipulated control) initial carbonate chemistry conditions. During each low-tide emersion period ($n = 23$), we randomly selected two or three pools in which we decreased pH to 7.5 at the start of the emersion. Following the low-tide emersion period, this was reversed, and pools that had been subject to present-day conditions in the previous low-tide emersion period were subject to future conditions and vice versa. However, due to diverse constraints, in 2 of the 23 emersion periods all the pools were left under present-day conditions.

In this experiment, we compared present and future seawater carbonate chemistry conditions. To simulate future carbonate chemistry conditions, we added small volumes of CO_2-enriched seawater (total of ~ 100–200 mL) at the start of the emersion period in 50 mL increments until the well-mixed pool water reached the desired pH levels (pH $= 7.5$, reached in less than 10 min). CO_2-enriched seawater was pre-
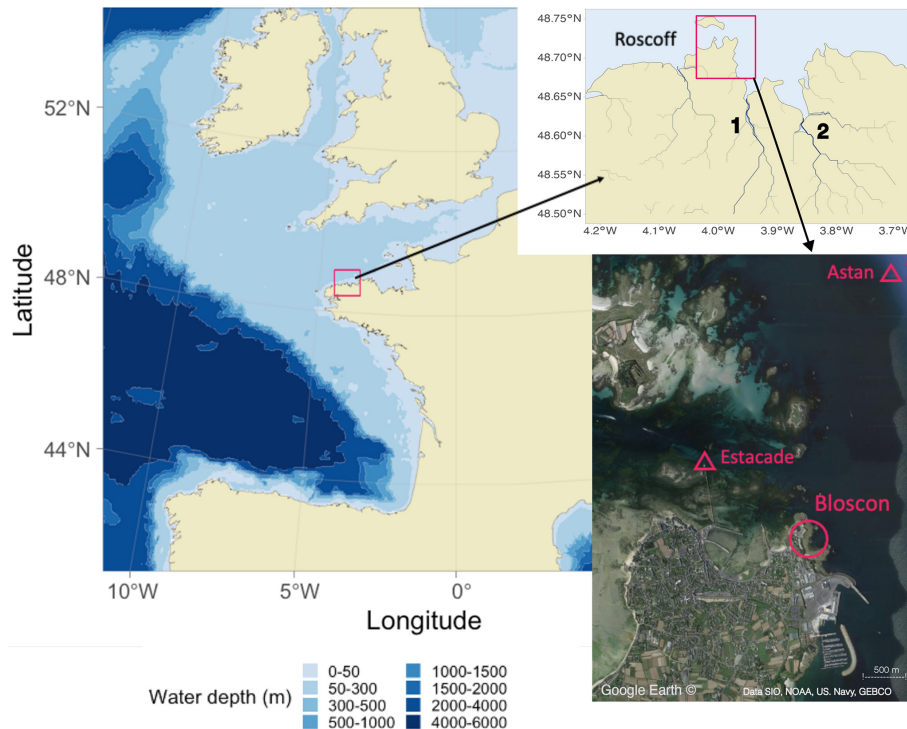
Figure 1. Field site location on a map of Europe (left). The study site (Bloscon) is located in Roscoff, Brittany, France (top right: river mapping data from *HydroSHEDS*, Penzé river and Morlaix river; bottom: satellite image from © Google Earth, https://earth.google.com/web/, acquired in June 2022). The SOMLIT stations Astan and Estacade are indicated with triangles (https://www.somlit.fr/en, last access: 1 June 2023).
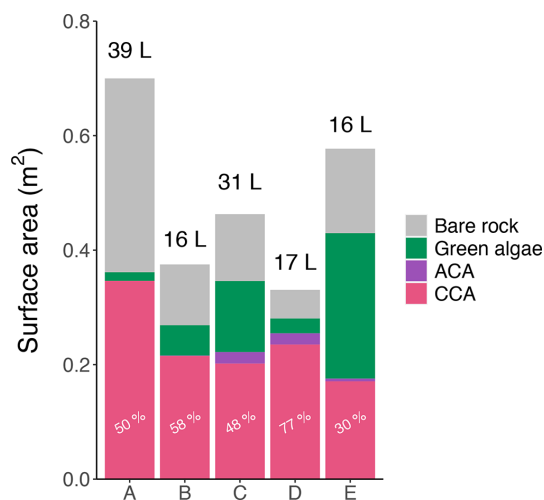

Figure 2. Pool area, volume and coverage. Surface of the five pools (A–E, September 2020) covered by crustose coralline algae (CCA, pink), articulated coralline algae (ACA, purple) and green algae (green) or free of algae (bare rock, gray). The length of the bars represents total pool surface area (m^2), and the volume of each pool (L) is indicated above. The relative coverage (%) of calcifying algae (ACA + CCA) in each pool is given. Details for the other seasons are available in Figs. SP1 and SP2 in the Supplement.

Table 1. Sampling schedule: the dates of each field session are presented. Pools were monitored throughout multiple low-tide emersion periods (diurnal and nocturnal).

Season	Dates	Low-tide emersion periods (N)	
		Diurnal	Nocturnal
Winter	14–17 February 2020	2	0
	9–19 February 2021	8	2
Spring	28–29 April 2021	2	0
Summer	2–11 September 2020	5	1
	6–9 September 2021	0	3

pared by supersaturating adjacent seawater in CO_2 using a high-pressure CO_2 cylinder.

2.4 Sampling and measurement of seawater parameters

Temperature, salinity, pH, oxygen and ammonium. From the start of the emersion period, we measured five parameters periodically using Hach Lange (Loveland, Colorado, USA) probes: temperature, pH$_T$ (IntelliCAL PHC101, accuracy:

±0.02 pH units), salinity (conductivity probe IntelliCAL CDC401, ±0.1 units), oxygen concentration (optical sensor IntelliCAL LDO101, accuracy: ±0.1 for 0 to $8\,\mathrm{mg\,L^{-1}}$, ±$0.2\,\mathrm{mg\,L^{-1}}$ for values greater than $8\,\mathrm{mg\,L^{-1}}$, maximum $22\,\mathrm{mg\,L^{-1}}$) and NH_4^+ concentration (ion-selective electrode IntelliCAL ISENH4181, range: 0.018–$9000\,\mathrm{mg\,L^{-1}}\ NH_4^+$–N). Pools were well mixed before any measurement to assure no influence of gradients forming in the pools. The measurement frequency during the emersion periods was every 15–20 min during the day ($n = 1392$) and reduced to once an hour at night ($n = 159$), when temperature, pH and light variations were limited or absent; pH was calibrated on the total scale (pH_T) using a TRIS (2-amino-2-hydroxy-1,3-propanediol) and AMP (2-aminopyridine) buffer solution with a salinity of 35.0, following the recommendations from Dickson et al. (2007).

Total alkalinity. Discrete samples for total alkalinity (TA) analysis were collected hourly. The average time between two samples was $1.0 \pm 0.2\,\mathrm{h}$ ($n = 492$, median = 1.0) during daytime and $1.4 \pm 0.9\,\mathrm{h}$ ($n = 135$, median = 1.0) during nighttime. Seawater (150 mL) was filtered with 0.7 µm GF/F borosilicates filters directly after sampling. These samples were stored in a dark cool box until the end of the tide (max. 7 h). Upon return to the lab, they were stored at 4 °C in the dark until they were either analyzed within the week or poisoned with 50 µL of saturated $HgCl_2$. TA was assessed potentiometrically using $50.0 \pm 0.5\,\mathrm{g}$ of seawater and a semi-automated titration system (0.1 M HCl, Titrino 848 plus by Metrohm, Switzerland; electrode calibrated on the National Bureau of Standards scale). TA was determined using Gran titration (Gran, 1952) according to the method of Haraldsson et al. (1997) and verified against reference standards provided by (Scripps Institute of Oceanography, University of California, San Diego, United States). TA samples were analyzed with single ($n = 312$) or duplicate ($n = 320$) measurements (the median of the standard deviation between duplicates was $1.05\,\mathrm{µmol\,kg^{-1}}$). TA was salinity-normalized before further calculations to take into account possible dilution from rain or concentration from evaporation.

To take into account the influence of the changes in nutrients (NO_3^-, NO_2^-, PO_4^{3-} and NH_4^+) on the changes in TA (Gazeau et al., 2015), we sampled seawater for nutrients in winter (February 2020) and summer (September 2020). Samples were taken during the day at the start and end of the emersion periods in the five pools. Around 60 mL of seawater was immediately filtered on 0.2 µm cellulose filters, stored in 125 mL polyethylene bottles in a cool dark box (max. 7 h) and then frozen at −20 °C until analysis. Nutrient concentrations were obtained using an AA3 auto-analyzer (Seal Analytical) using the method from Aminot and Kérouel (2007). Changes in nutrient concentrations were near-negligible contributions to TA changes throughout a low-tide emersion period ($< 6\,\mathrm{µmol\,kg^{-1}}$, i.e., $< 2\,\%$ of the observed change in TA; see full details in "Nutrients" in the Supplement) and thus are ignored here.

Light measurements. Surface irradiance (photosynthetically active radiation, PAR) was continuously recorded (every minute) during experiments at the field station using a LI-COR flat quantum light sensor (LI-190R) and logger (LI-1500, LI-COR, Germany).

Adjacent waters. Temperature, salinity, pH and TA ($n = 5$) were similarly sampled and measured at the sampling site during ebb tide for the three seasons.

2.5 Carbonate chemistry calculations

The carbonate system parameters (e.g., pCO_2; DIC concentration; CO_3^{2-} concentration; and Ω_a, the aragonite saturation state) were calculated from the measurements of pH_T, TA, temperature and salinity using the *R* package *seacarb* (Gattuso et al., 2021) with the default dissociation constants recommended by Dickson et al. (2007), except for the low temperatures encountered in February 2021, where the refined constants of Sulpis et al. (2020) were used. When salinity decreased by more than 1.5 units h^{-1}, data were excluded to avoid rain effects in the present study. When calculated DIC and Ω_a were negative, likely due to inaccuracies in the measurement and computation of the carbonate system, values were approximated to be 0 (7/627 values). The air–sea gas fluxes due to net diffusive transport were considered to be negligible in the pools (see detailed explanation the interactive discussion).

2.6 Biological activity calculations

The rates of net community calcification (NCC; mmol $CaCO_3\,\mathrm{m^{-2}\,h^{-1}}$) and net community production (NCP) or community respiration (CR; mmol $O_2\,\mathrm{m^{-2}\,h^{-1}}$ or mmol $C\,\mathrm{m^{-2}\,h^{-1}}$) were calculated between two consecutive sampling times. These rates respectively represent the measured changes in net $CaCO_3$ precipitation and net organic carbon production (or oxygen consumption) by the community. Positive NCC represents net $CaCO_3$ precipitation (gross precipitation > dissolution), and negative rates represent net dissolution (dissolution > precipitation). NCP is positive when the community primary production exceeds respiration and negative when community primary production is less than respiration. We use CR for nights, when there is no primary production (oxygen consumption and carbon release only).

NCC was calculated using the alkalinity anomaly method (Smith and Key, 1975). Briefly, for each mole of $CaCO_3$ precipitated, 2 mol of HCO_3^- combine with Ca^{2+}, and TA decreases by 2 mol (Eq. 1). Two independent estimates of NCP (or CR) were calculated, one derived from changes in ΔO_2 (NCP_{O_2} or CR_{O_2}) and one derived from ΔDIC and NCC (NCP_{DIC} or CR_{DIC}).

NCC and NCP (or CR) were thus calculated as follows:

$$NCC = \frac{-\Delta TA}{2\Delta t} \times \frac{V}{S} \qquad (1)$$

$$NCP(\text{or CR})_{O_2} = \frac{\Delta O_2}{\Delta t} \times \frac{V}{S} \qquad (2)$$

$$NCP(\text{or CR})_{DIC} = \frac{-\Delta DIC}{\Delta t} \times \frac{V}{S} - NCC, \qquad (3)$$

with ΔTA (mmol L^{-1}), ΔDIC (mmol L^{-1}) and ΔO_2 (mmol L^{-1}) the change in concentration of TA, DIC and O_2 between consecutive samples and Δt the duration between consecutive samples (h), V the pool volume (L) and S the pool surface area (m^2).

Up to seven NCC and NCP (or CR) rates were calculated for each pool during each emersion period (one per hour). These rates were used to investigate the direct correlation between biological activity and environmental factors such as light intensity or Ω_a.

Rates calculated this way are however not independent from each other (i.e., the rate measured at $t + 2$ is dependent on the rate at $t + 1$), limiting further statistical analyses of the effect of the treatment. This is why, to investigate the effect of pH treatment (present vs. future) on community biological activity, we also calculated NCC and NCP or CR using linear regressions (NCC_{lm} and NCP_{lm} or CR_{lm}) between TA, [DIC] and [O_2] and time after the start of the emersion period (for detailed results of the regressions, e.g., goodness of fit, see LM1-3 in the Supplement). The few data from diurnal tides that were taken after sunset were excluded from these regressions. For oxygen, data were limited to the first 3 h of emersion as high O_2 concentrations ($> 22 \text{ mg L}^{-1}$) and supersaturation ($> 200\%$) led to inaccurate measurements and/or possible oxygen degassing afterwards (see LM2 in the Supplement). This regression approach provides a single estimate of the rate of NCC, NCP_{DIC} (or CR_{DIC}) and NCP_{O_2} (or CR_{O_2}) for each pool during each emersion period ($n = 17$ diurnal and 6 nocturnal low-tide emersion periods $\times$ 5 pools $= 115$). These rates were then used in generalized linear mixed models (GLMMs) to assess the effect of pH treatment on diurnal and nocturnal biological activity (see "Statistical analyses" below).

We calculated community calcification budget and production budget (respectively CCB and CPB) at emersion as an indication of the night–day balance in calcification and production: when CCB (CPB) is positive, the pool community calcifies (produces) more by day than it dissolves (respires) at night. Both were calculated for winter (February 2020 and 2021) and summer (September 2020 and 2021) for each pool as follows:

$$CCB = NCC_D + NCC_N \qquad (4)$$

$$CPB = NCP_D + CR_N, \qquad (5)$$

with NCC_D and NCP_D (> 0) the average diurnal NCC and NCP for a given pool for a treatment and a season and NCC_N and CR_N (< 0) the average nocturnal NCC and dark respiration for the same conditions. Three approaches were used for estimating CPB, given the uncertainties in each NCP estimate (see Discussion): (1) O_2-derived estimates of NCP (CPB_{O_2}), (2) DIC-derived estimates (CPB_{DIC}), and (3) a "mixed" approach that combined nocturnal CR_{O_2} and diurnal NCP_{DIC} (CPB_m) under the assumption that 1 mol of carbon is produced/consumed when 1 mol of O_2 is produced/consumed. Although CPB resembles gross community production in the way the rates are calculated (difference between light and dark net production/respiration rates), if one wanted to reuse these rates for gross community production, they should do so with care due to differences in night and day temperature (see extended discussion on this subject in Bracken et al., 2022). The treatment effect was assessed on CCB and CPB by comparing the change due to the future treatment in each pool.

2.7 Statistical analyses

All data are presented as mean $\pm$ standard deviation (SD). The analyses were made using the software R (R Core Team, 2017). The level of significance used was 5 %. Because data were measured in the same five pools but on different days for different treatments, we used GLMM to test for the effect of treatment on NCC_{lm} and on O_2 and DIC-derived NCP_{lm} (or CR_{lm}), assigning sampling days (i.e., low-tide emersion periods) as the random factor and pools (five levels), mean temperature of the pool during low-tide emersion period (a continuous proxy for season) and treatment (treat: future vs. present) as fixed factors. This was performed using the *R* package *nlme* (Pinheiro et al., 2018). Models with and without standardized residuals were compared using analyses of variance (ANOVAs), and, when different, the Akaike information criterion (AIC) was used to choose the best-fitted model of the two. For GLMMs, mean daily PAR was not used as it has strong collinearity with mean daily temperature/season. We used ANOVAs to test the effect of temperature, pool and treatment on initial (averaged over the first hour of emersion) and final (averaged for > 5 h after emersion) carbonate chemistry conditions. The normality of the data was tested using Shapiro–Wilk tests and qq plots, while variance homogeneity was tested with Bartlett tests.

3 Results

3.1 Environmental conditions

Adjacent waters. Temperatures (and salinity) measured in the seawater adjacent to the pools were 6–7 °C in winter (February; salinity $S = 35.0$), 11–12 °C in spring (April; $S = 35.5$) and 17–18 °C in summer (September; $S = 36.0$). This seawater was characterized by an average pH_T of 8.01 ± 0.06 units, total alkalinity of $2319 \pm 6\,\mu\text{mol kg}^{-1}$, $p\text{CO}_2$ of

$445 \pm 69\,\mu\text{atm}$, Ω_a of 2.2 ± 0.3 and $[O_2]$ of $100 \pm 1\,\%$ of air saturation (or $10.1 \pm 1.5\,\text{mg L}^{-1}$; $n = 5$).

Light duration and intensity. In Roscoff, day–night (i.e., no light) periods are typically 10 h of day, 14 h of night in February and 14 h of day, 10 h of night in April and September. Photosynthetically active radiation (PAR) was 2 to 3 times higher in spring/summer (April/September $\sim 1500\,\mu\text{mol m}^{-2}\,\text{s}^{-1}$; Fig. 3a) than in winter (February $\sim 500\,\mu\text{mol m}^{-2}\,\text{s}^{-1}$).

Carbonate chemistry conditions at the start of the emersion period ($< 1\,h$ post-emersion). For both diurnal and nocturnal tides, the initial pH was significantly lower in pools with added CO_2 than in the present-day pools ($\text{pH}_T = 8.2 \pm 0.1$ vs. 7.5 ± 0.2 units during the day and 8.0 ± 0.1 vs. 7.4 ± 0.1 units at night for present and future pools respectively; treat: $p < 0.001$; detailed results in Figs. S2–S3, Table S1–S2). This corresponds to pCO_2 of 260 ± 100 vs. $1900 \pm 835\,\mu\text{atm}$ (day) and 510 ± 90 vs. $2310 \pm 410\,\mu\text{atm}$ (night) for pools under present and future conditions respectively. Adding CO_2 in the pools increased the mean DIC concentration by $320\,\mu\text{mol kg}^{-1}$ during the day and $240\,\mu\text{mol kg}^{-1}$ during the night. Under present-day conditions, the pools started at supersaturated levels with regard to aragonite (day: $\Omega_a = 3.3 \pm 1.3$; night: 2.2 ± 0.3). Adding CO_2 significantly decreased Ω_a (treat: $p < 0.001$; Table S1), leading to initial future conditions often undersaturated with regard to aragonite ($\Omega_a = 0.8 \pm 0.5$) by day and always undersaturated conditions by night ($\Omega_a = 0.6 \pm 0.1$). Furthermore, under future diurnal conditions, pools were always undersaturated with respect to aragonite from the start of the emersion period in February ($\Omega_a = 0.5 \pm 0.2$) but not in April ($\Omega_a = 1.1 \pm 0.7$) and September ($\Omega_a = 1.2 \pm 0.5$; Table S1). At the start of emersion, total alkalinity was $2303 \pm 34\,\mu\text{mol kg}^{-1}$ (similar to adjacent seawater) and uncorrelated with treatment ($p > 0.05$) and temperature ($p > 0.6$).

As data were averaged on the first hour post-emersion; the mean initial oxygen concentration calculated was already affected by NCP by day ($14.0 \pm 2\,\text{mg O}_2\,\text{L}^{-1}$) and CR by night ($9.5 \pm 1.5\,\text{mg O}_2\,\text{L}^{-1}$ vs. $10.1 \pm 1.5\,\text{mg O}_2\,\text{L}^{-1}$ for adjacent seawater). This was also visible in CO_2 partial pressure, with lower pCO_2 than expected during the first hour post-emersion by day ($262 \pm 102\,\mu\text{atm}$ vs. $445 \pm 69\,\mu\text{atm}$ for adjacent seawater) and higher pCO_2 at night ($508 \pm 88\,\mu\text{atm}$) under the present-day conditions.

3.2 Diurnal tides

Diurnal pool chemistry. Starting from the aforementioned values at emersion, the pools followed a clear temporal evolution due to solar irradiance and community metabolism (Fig. 3). Firstly, we observed increases in salinity ($+1.5$ units on average; Fig. 3a) and temperature ($+4\,°\text{C}$ in September, $+6\,°\text{C}$ in April on average) in summer and spring. In winter, temperatures tended to decrease ($-1.7\,°\text{C}$ on average), with air temperatures colder than that of the seawater; salinity was stable (35.5 ± 0.8).

Secondly, we observed positive NCP, corroborated by a doubling in oxygen concentration (Fig. 3a) a few hours after the start of emersion. In parallel, the seawater DIC concentration decreased by $50\,\%$ from the initial concentration (from 2130 ± 195 to $1140 \pm 560\,\mu\text{mol kg}^{-1}$; Fig. 3b), the range of which largely depended on the season (Fig. S2). For instance, in February, DIC consumption in pool seawater averaged $\sim 700\,\mu\text{mol kg}^{-1}$ over a low-tide period, while it averaged $\sim 1500\,\mu\text{mol kg}^{-1}$ in September. Particularly extreme conditions, with DIC concentrations effectively reaching $0\,\mu\text{mol kg}^{-1}$, were observed in two of the pools at three tides in September 2020 (see further details below in "The particular case of September 2020 tides"). At the end of diurnal emersions, average pCO_2 was always below $100\,\mu\text{atm}$, reaching as low as $1 \pm 2\,\mu\text{atm}$ in September (Fig. 3b, Table S1). As a result, diurnal pH_T increased to 9.1 ± 0.6 by the end of emersion, with maximum values up to 10.3 in summer (Fig. 3b). At the end of a diurnal emersion period, the pools' pH was stable, either reaching a plateau or decreasing after sunset (see PAR in Fig. 3a). Similarly, at the end of diurnal emersion periods, Ω_a was high (5.6 ± 3.0 on average, max 10.4). Lastly, we observed a diurnal decrease in TA by $415\,\mu\text{mol kg}^{-1}$ on average, indicative of net calcification.

It is noteworthy that the carbonate chemistry conditions experienced at the end of diurnal emersion converged whatever the initial treatment (Fig. S2, Table S1). For instance, while Ω_a was significantly different between treatments at the start of the emersion period, both treatments reached similar Ω_a at the end of emersion ($> 5\,h$) of around 5.3 ± 2.2 (ANOVA: treat – $p = 0.1$, temp – $p = 0.002$, pool – $p = 0.01$). There was less convergence for pH_T; even 5 h after emersion, the treatments were still statistically significant, although the differences in pH were small ($p < 0.001$ for pH_T with 9.2 ± 0.6 for present and 9.0 ± 0.6 for future pools).

Diurnal biological activity. Net community production was positive during daytime, except at sunset (Fig. 3c). NCP was significantly correlated with light intensity (PAR), and further results for hourly NCP and their correlation with hourly averaged PAR, Ω_a and temperature can be found in the Supplement (Figs. S6 and S7).

As expected, seasons/temperature affected net oxygen production (O_2-derived NCP_{lm}), increasing from $7 \pm 3\,\text{mmol O}_2\,\text{m}^{-2}\,\text{h}^{-1}$ in February to $18 \pm 11\,\text{mmol O}_2\,\text{m}^{-2}\,\text{h}^{-1}$ in September (GLMM, $p < 0.001$; Fig. 4a and Table 2A). CO_2 addition increased O_2-derived NCP_{lm} by $20\,\%$ on average over all seasons, from $10 \pm 7\,\text{mmol O}_2\,\text{m}^{-2}\,\text{h}^{-1}$ under present conditions to $12 \pm 9\,\text{mmol O}_2\,\text{m}^{-2}\,\text{h}^{-1}$ ($p = 0.0015$). Net oxygen production differed across pools ($p < 0.003$), with significantly more productivity in Pools C ($17.6 \pm 12.7\,\text{mmol O}_2\,\text{m}^{-2}\,\text{h}^{-1}$) and D
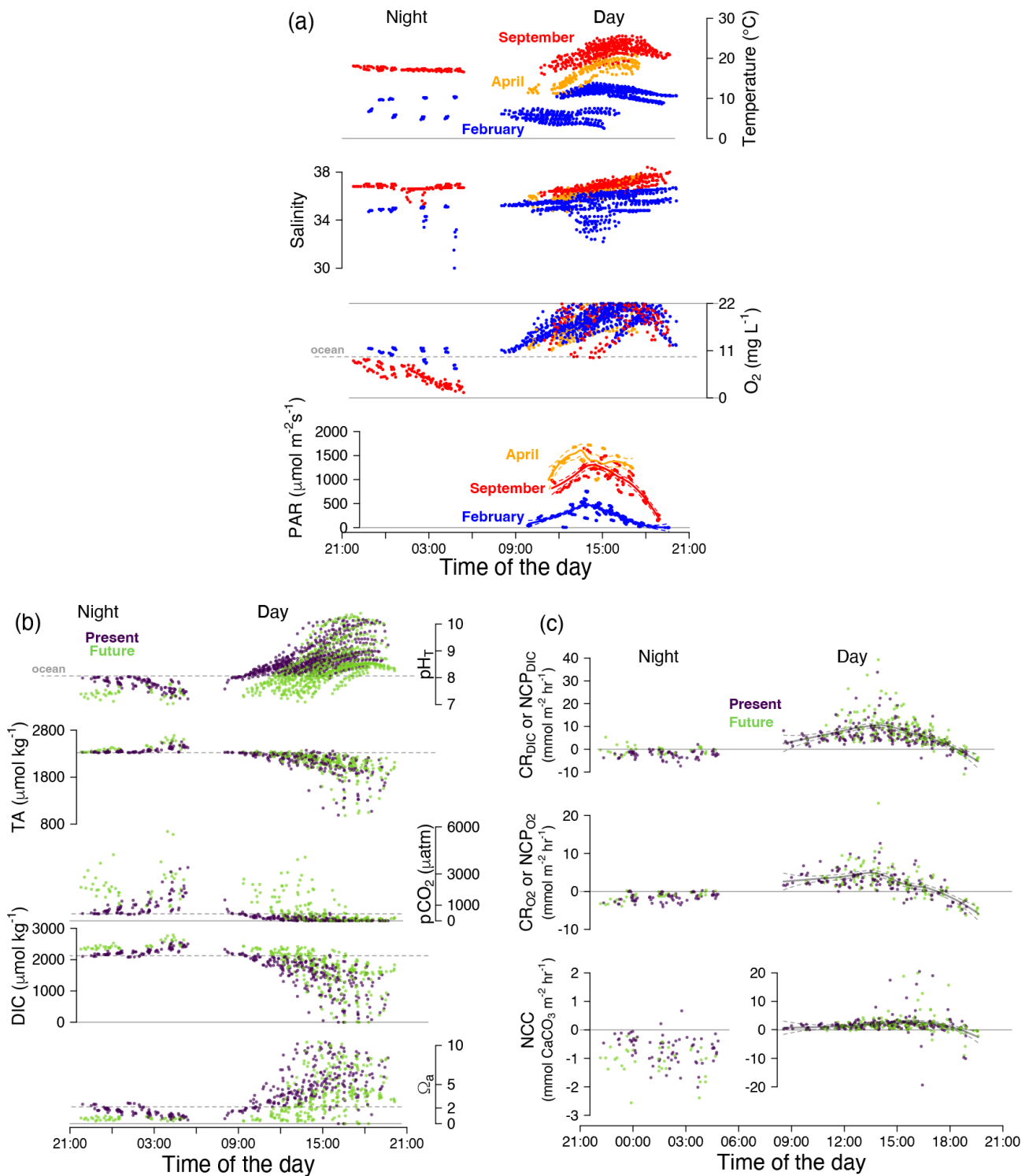
Figure 3. Composite 24 h conditions and biological activity for all pools. **(a)** Temperature (°C), salinity and oxygen concentration (mg L^{-1}) and photosynthetically active radiation (PAR; µmol m^{-2} s^{-1}); **(b)** pH$_T$, total alkalinity (TA; µmol kg^{-1}), pCO$_2$ (µatm), dissolved inorganic carbon (DIC; µmol kg^{-1}) and aragonite saturation state (Ω_a); and **(c)** DIC- and O$_2$-derived NCP or CR (mmol C or O m^{-2} h^{-1}) and NCC (mmol CaCO$_3$ m^{-2} h^{-1}). Colors represent seasons (**a**: blue for February, orange for April, red for September) and treatment (**b** and **c**: purple for present and green for future). Horizontal dotted gray lines represent the mean values of the adjacent ocean. Curves were fitted by season for PAR and for diurnal NCP and NCC using a local polynomial regression (LOESS) with a 95 % confidence interval. Number of observations: $n = 1551$ for temperature, salinity and pH$_T$; $n = 1169$ for oxygen concentration (data recorded < 22 mg L^{-1}); and $n = 632$ (hourly data) for the carbonate chemistry parameters NCC and NCP or CR **(b)**. All pools are shown.

$(10.6 \pm 5.6 \, \text{mmol} \, O_2 \, \text{m}^{-2} \, \text{h}^{-1})$ compared to Pools A, B and E $(8.1 \pm 4.1 \, \text{mmol} \, O_2 \, \text{m}^{-2} \, \text{h}^{-1})$.

Results are similar for DIC-derived NCP_{lm} (Fig. 4a and Table 2b), with primary production ranging from $6 \pm 2 \, \text{mmol} \, C \, \text{m}^{-2} \, \text{h}^{-1}$ in February to up to $12 \pm 5 \, \text{mmol} \, C \, \text{m}^{-2} \, \text{h}^{-1}$ in September $(p < 0.001)$. As for O_2-derived NCP_{lm} CO_2 addition increased DIC-derived NCP_{lm} by 20 % on average over all seasons $(p < 0.001;$ Fig. 4a). This increase was particularly apparent in the summer, when NCP_{lm} increased from $11 \pm 4 \, \text{mmol} \, \text{m}^{-2} \, \text{h}^{-1}$ in the present treatment to $15 \pm 5 \, \text{mmol} \, C \, \text{m}^{-2} \, \text{h}^{-1}$ in the future treatment $(+35 \%)$. Productivity (NCP_{lm}) was significantly lower in Pools B and E than in Pool A and significantly higher in Pools C and D $(p < 0.003)$.

By day, with the exception of sunset, net community calcification was positive (NCC and $\text{NCC}_{\text{lm}} > 0$; Figs. 3c and 4b) and occurred in an environment that was supersaturated with regard to aragonite (Fig. 3b). This was with the exception of a few emersion periods in September 2020 where dissolution was observed despite high-saturation-state conditions (further details below). Similar to NCP_{lm}, diurnal net calcification rates (NCC_{lm}) were strongly influenced by temperature/season (GLMM, $p < 0.001$; Fig. 4b and Table 2c), ranging from $1.2 \pm 0.5 \, \text{mmol} \, CaCO_3 \, \text{m}^{-2} \, \text{h}^{-1}$ in February to $3.3 \pm 1.3 \, \text{mmol} \, CaCO_3 \, \text{m}^{-2} \, \text{h}^{-1}$ in September. NCC hourly rates positively correlated with averaged Ω_a $(p < 0.0001, \text{NCC} = 0.15 \times \Omega_a + 0.85$; linear regression presented in Fig. S7) significantly but not strongly $(R^2 = 10 \%)$. CO_2 addition did not influence NCC_{lm} rates during the day $(p = 0.47)$. However, NCC_{lm} did differ across pools $(p < 0.003)$: rates were relatively low in Pool E (lowest CCA cover: 30 %; $1.4 \pm 1.4 \, \text{mmol} \, CaCO_3 \, \text{m}^{-2} \, \text{h}^{-1}$) and high in Pool D (highest CCA cover: 70 %; $2.2 \pm 0.8 \, \text{mmol} \, CaCO_3 \, \text{m}^{-2} \, \text{h}^{-1}$) compared to the three other pools $(2.0 \pm 1.25 \, \text{mmol} \, CaCO_3 \, \text{m}^{-2} \, \text{h}^{-1})$.

3.3 Nocturnal tides

Nocturnal pool chemistry. Seawater temperatures during the nights were stable (Fig. 3a) throughout the emersion period in summer (from $17.3 \pm 0.4 \, ^\circ\text{C} < 1 \, \text{h}$ post-emersion to $17.2 \pm 0.2 \, ^\circ\text{C} > 5 \, \text{h}$ post-emersion) and winter (from 8.4 ± 1.4 to $7.8 \pm 2.7 \, ^\circ\text{C}$ in February; no April nights). We highlight the wide range of winter seawater temperatures with an exceptionally cold tidal cycle ($5 \, ^\circ\text{C}$ on 13 February 2021) due to air temperatures of 3–$4 \, ^\circ\text{C}$ (observations from the Île de Batz meteorological station). There was a decline in salinity at night in some winter emersion periods (Fig. 3a) due to high air humidity and/or rain. Data where salinity dropped by more than 1.5 units in less than an hour were removed from further analyses of net community calcification and respiration.

After 5 h of emersion, O_2 concentration had decreased by 50 % (from $10.1 \pm 1.5 \, \text{mg} \, O_2 \, \text{L}^{-1}$ to $4.9 \pm 3.3 \, \text{mg} \, O_2 \, \text{L}^{-1}$) (Fig. 3a) due to community respiration. Simultaneously, pH_{T}

decreased to 7.6 ± 0.2 (present) or stayed at 7.4 ± 0.2 (future; Figs. 3b and S2, Table S1), with significant effects of pools, treatment and temperature $(p < 0.001$ for all three). DIC concentration increased by $+256 \, \mu\text{mol} \, \text{kg}^{-1}$ on average over an emersion period. The range of this increase depended on the temperature and the pool: in winter $(5$–$10 \, ^\circ\text{C})$, present-day pool seawater gained $+130 \, \mu\text{mol} \, \text{kg}^{-1}$ $(+60$ for future pools) of DIC over an emersion period, when in summer it gained $+370 \, \mu\text{mol} \, \text{kg}^{-1}$ for present (future: $+310 \, \mu\text{mol} \, \text{kg}^{-1}$) pools (Fig. S3). Saturation state converged towards similar undersaturated levels at night (Figs. 3b and S2, Table S1): Ω_a stayed stable in the future treatment $(0.7 \pm 0.2$ units on average) and decreased in the present-day treatment $(-1.2$ units from initial Ω_a). At the end of nocturnal emersion Ω_a values were still statistically different due to the initial treatment $(p < 0.001$ for treat, temp and pools).

Nocturnal biological activity. At night, oxygen was consumed; i.e., we observed dark respiration (CR; Fig. 3c). Community respiration $(O_2$-derived $\text{CR}_{\text{lm}})$ varied according to season $(p < 0.001$; Fig. 4a and Table 2a): temperature linearly increased nocturnal respiration rates from $-1.0 \pm 1.2 \, \text{mmol} \, O_2 \, \text{m}^{-2} \, \text{h}^{-1}$ in February to $-4.7 \pm 1.3 \, \text{mmol} \, O_2 \, \text{m}^{-2} \, \text{h}^{-1}$ in September. The CO_2 treatment did not influence night respiration $(p = 0.39)$. Respiration rates were significantly influenced by pools $(p = 0.03)$, probably linked to the relative biomass of heterotrophs and autotrophs; respiration was significantly higher in Pool C $(-4.6 \pm 2.8 \, \text{mmol} \, O_2 \, \text{m}^{-2} \, \text{h}^{-1})$ and significantly lower in Pool E $(-2.4 \pm 1.4 \, \text{mmol} \, O_2 \, \text{m}^{-2} \, \text{h}^{-1})$ than in Pools A, B and D $(-3.4 \pm 2.1 \, \text{mmol} \, O_2 \, \text{m}^{-2} \, \text{h}^{-1})$.

Night respiration estimated using DIC and NCC was near zero $(\text{CR}_{\text{lm}} = -0.2 \pm 0.7 \, \text{mmol} \, \text{m}^{-2} \, \text{h}^{-1})$. At these low rates, uncertainties associated with much higher rates of net dissolution (negative NCC) sometimes led to spuriously positive DIC-derived CR estimates, hindering interpretation. Nevertheless, DIC-derived community respiration was 10 times lower in February than in September $(-0.2 \pm 0.7$ and $-2.3 \pm 1.1 \, \text{mmol} \, C \, \text{m}^{-2} \, \text{h}^{-1}$ respectively), although it was not linearly driven by temperature $(p = 0.053$; Fig. 4B and Table 2B). Adding CO_2 to the pools influenced DIC-derived community respiration in a way that was inverse to that seen with O_2, but as stated above, this was likely an artifact of subtracting NCC from small DIC changes. As for O_2, DIC-derived CR_{lm} significantly changed depending on the pools.

At night, the pools experienced significant net community dissolution $(\text{NCC} < 0$; Fig. 3c) even when waters were supersaturated with regard to aragonite in the present treatment $(\Omega_a > 1$; Fig. 3b). Nocturnal net dissolution rates (NCC_{lm}) were not significantly affected by temperature in the range investigated $(5$–$18 \, ^\circ\text{C}, p = 0.57$; Fig. 4c and Table 2c). However, adding CO_2 in the pools increased net dissolution rates $(p = 0.0017)$ from $-0.7 \pm 0.3 \, \text{mmol} \, CaCO_3 \, \text{m}^{-2} \, \text{h}^{-1}$ to $-1.0 \pm 0.4 \, \text{mmol} \, CaCO_3 \, \text{m}^{-2} \, \text{h}^{-1}$ $(+40 \%)$. Similarly, looking instead at hourly rates (NCC), dissolution correlated significantly $(p < 0.0001)$ with Ω_a $(\text{NCC} = 0.34 \times \Omega_a$

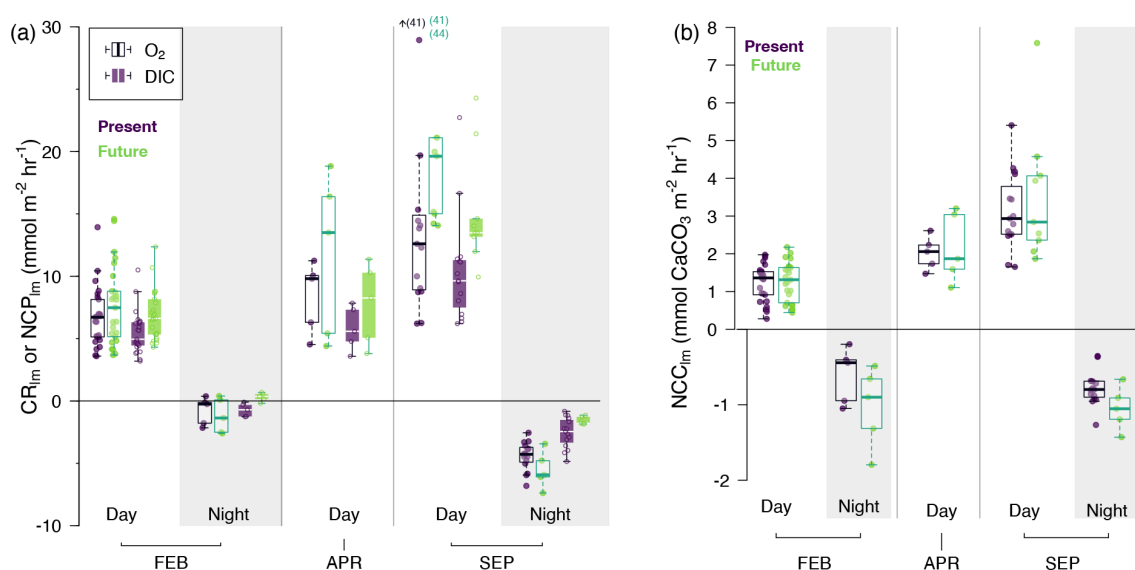**Figure 4. (a)** O_2-derived (white boxes) and DIC-derived (colored boxes) NCP_{lm} (mmol m^{-2} h^{-1}) and **(b)** NCC_{lm} (mmol CaCO$_3$ m^{-2} h^{-1}) during the day and night (shaded areas) by season and by treatment (purple for present and green for future); rates are presented as boxplots showing median, first and third quartile, and 1.5 inter-quartile range (bars) with overlain individual observations (round symbols). Individual rates were calculated for each pool, each tide and each treatment: $n = 50$ (FEB, day), $n = 10$ (FEB, night), $n = 10$ (APR, day), $n = 25$ (SEP, day), $n = 20$ (SEP, night). Seasons: FEB for winter (pooled February 2020 and 2021), APR for spring (April 2021) and SEP for summer (pooled September 2020 and 2021). Note that for NCC_{lm}, nights (< 0) and days (> 0) have different y-axis scales for better visualization of night differences. Statistical details of the linear regressions can be found in the corresponding Supplement. For O_2-derived NCP_{lm}, in September, three rates were out of the range plotted, and their values are indicated next to the small arrow.

– 1.22, $R^2 = 11\%$; Fig. S7). The strength of this correlation depended on seasons and pools (Fig. S8). Net dissolution rates (NCC_{lm}) significantly differed by pool ($p < 0.0017$): the lowest rates were observed in Pool E (-0.4 ± 0.2 mmol CaCO$_3$ m^{-2} h^{-1}) – the pool with the lowest CCA cover – and the highest dissolution in Pool D – the pool with the highest CCA cover (-1.0 ± 0.4 vs. -0.9 ± 0.3 mmol CaCO$_3$ m^{-2} h^{-1} for A, B and C).

3.4 Influence of the treatment on CPB and CCB

Pools fixed more carbon during the day than they respired at night; i.e., the community production budget (CPB: balance between night and day) was positive in all the pools, in both winter and summer and whatever the treatment (Fig. 5). CPB$_{DIC}$ and CPB$_m$ estimates were typically lower than CPB$_{O_2}$ (in 14/20 cases and 18/20 cases respectively). The production budget was significantly lower in winter than in summer (FEB: CPB$_{O_2}$ = 3 ± 1 mmol O_2 m^{-2} h^{-1}; SEP: 7 ± 5 mmol O_2 m^{-2} h^{-1}; $t = -2.4$, d$f = 9.8$, $p = 0.03$). Adding CO_2 increased CPB in all the pools in summer by $+ 3.0 \pm 2.1$ mmol O_2 m^{-2} h^{-1}, an increase in production by 50% to 80% (ΔCPB; Fig. 5). In winter, there was no evidence of such a "fertilization effect" across the most accurate CPB estimates for this season (CPB$_{O_2}$, CPB$_m$): we only observed a significant increase in production due to CO_2 addition in two of the pools ($+60\%$ to $+120\%$ for A and B). For

the three other pools, CPB induced either minimal changes ($< 20\%$ for C and E) or a decrease in production (D: down to -34%). DIC-derived ΔCPB in winter (all positive) should be interpreted with caution since some nocturnal CR$_{lm}$ values were spuriously positive in the future treatment (see "Nocturnal biological activity" above).

The pools calcified more during the day than they dissolved at night (CCB > 0), in both summer and winter (Fig. 5). CCB was significantly lower in winter than in summer (FEB: CCB = 0.2 ± 0.2 mmol CaCO$_3$ m^{-2} h^{-1}; SEP: 1.2 ± 0.6 mmol CaCO$_3$ m^{-2} h^{-1}; $t = -5.2$, d$f = 11.7$, $p = 0.0002$). In winter, adding CO_2 decreased CCB by more than 80% in Pools C, D and E (Fig. 5). The CO_2 addition even resulted in a transition from a positive community calcification balance to dissolution in Pool C (133% change, from $+0.5$ to -0.2 mmol CaCO$_3$ m^{-2} h^{-1}). For the two other pools (A and B), winter CO_2 addition increased their relatively small calcification balance (A: $+87\%$, from 0.1 to 0.2 mmol CaCO$_3$ m^{-2} h^{-1}; B: $+71\%$, from 0.2 to 0.3 mmol CaCO$_3$ m^{-2} h^{-1}). In summer, changes in CCB due to treatment appeared minimal in Pools A, B and E ($< 15\%$ change) and either increased (C: $+67\%$) or decreased (D: -57%) in the two other pools.

Table 2. Results of the generalized linear mixed-effect models for **(a)** O_2-derived NCP_{lm} ($\text{mmol O}_2\,\text{m}^{-2}\,\text{h}^{-1}$), **(b)** DIC-derived NCP_{lm} ($\text{mmol C m}^{-2}\,\text{h}^{-1}$) and **(c)** NCC_{lm} ($\text{mmol CaCO}_3\,\text{m}^{-2}\,\text{h}^{-1}$) during the day and night. The models include three fixed factors – temp (mean temperature, a continuous factor), treat (for CO_2 future treatment vs. present, two levels) and pools (vs. Pool A, five levels) – and one random effect (low-tide emersion period or the calendar day on which the pool was measured). Significant p values are highlighted in bold.

(a)	O_2-derived NCP_{lm}		Estimate	Standard error	p value
Day	Intercept		1.49	1.37	0.28
	Fixed effects	Temp	0.54	0.13	**< 0.001**
		Treat	1.09	0.33	**0.0015**
		Pools	A, B, E ≠ C, D		**< 0.003**
	Random effect	Low-tide emersion period	8.90	0.90	**< 0.001**
Night	Intercept		2.87	0.98	**0.005**
	Fixed effects	Temp	−0.43	0.06	**< 0.001**
		Treat	−0.25	0.28	0.39
		Pools	A, B, D ≠ C, E		**< 0.03**
	Random effect	Low-tide emersion period	−3.46	0.87	**< 0.001**
(b)	DIC-derived NCP_{lm}		Estimate	Standard error	p value
Day	Intercept		2.3	1.08	**0.035**
	Fixed effects	Temp	0.38	0.08	**< 0.001**
		Treat	1.25	0.25	**< 0.001**
		Pools	A ≠ B, C, D, E		**< 0.003**
	Random effect	Low-tide emersion period	7.7	0.7	**< 0.001**
Night	Intercept		−0.94	1.4	0.51
	Fixed effects	Temp	−0.92	0.19	0.053
		Treat	−0.25	0.28	**< 0.001**
		Pools	A, B, D, E ≠ C		**0.016**
	Random effect	Low-tide emersion period	1.61	0.57	**0.01**
(c)	NCC_{lm}		Estimate	Standard error	p value
Day	Intercept		−0.16	0.31	0.61
	Fixed effects	Temp	−0.13	0.02	**< 0.001**
		Treat	0.06	0.08	0.47
		Pools	A, B, C ≠ D, E		**< 0.003**
	Random effect	Low-tide emersion period	−1.90	0.24	**< 0.001**
Night	Intercept		0.64	0.26	**0.026**
	Fixed effects	Temp	0.009	0.016	0.57
		Treat	0.28	0.07	**0.0017**
		Pools	A, B, C ≠ D, E		**< 0.017**
	Random effect	Low-tide emersion period	0.83	0.078	**< 0.001**

3.5 The particular case of September 2020 tides

During diurnal tides of September 2020 (high-PAR and high-temperature summer conditions), we observed an unexpected phenomenon: dissolution occurred at extremely high pH_T values (9–10) in Pools C and E (Fig. 6). Under these conditions effectively all the seawater DIC in these pools was consumed by photosynthesis and calcification (DIC $\approx 0\,\text{mmol kg}^{-1}$) 4 h after emersion. As such, the CO_3^{2-} concentration was also effectively zero, and the pools reached very low saturation states ($\Omega_a \approx 0$) despite high pH (Fig. 6). These conditions were quickly followed by indicators of $CaCO_3$ dissolution (increasing TA and DIC) instead of the expected diurnal precipitation. It is therefore notewor-
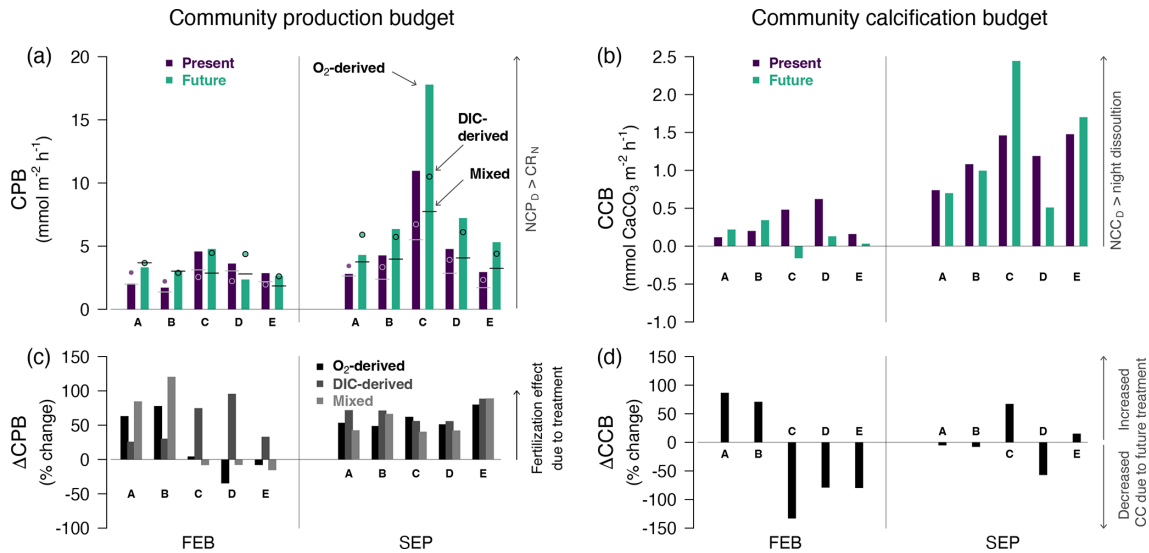
Figure 5. Community production budget (CPB[1]) **(a)** and calcification budget (CCB; $mmol\,CaCO_3\,m^{-2}\,h^{-1}$) **(b)** by treatment (purple for present and green for future) for each pool and season (same legend as Fig. 4). CPB > 0 if diurnal NCP > nocturnal respiration, and CCB > 0 if diurnal NCC > nocturnal dissolution. CPB was estimated three different ways: from O_2-derived NCP (bars), from DIC-derived NCP (round symbols) and from nocturnal O_2-derived CR combined with diurnal DIC-derived NCP (mixed, vertical segments). Panels **(c)** and **(d)** present the change (%) in diel production (ΔCPB, **a, c**) and diel calcification (ΔCCB, **b, d**) due to CO_2 addition. Positive ΔCPB indicates a fertilization effect due to the CO_2 addition; negative ΔCCB is expected if the CO_2 addition decreases net calcification/increases net dissolution. All three methods to estimate CPB indicate a fertilization effect in summer.

thy that dissolution may happen at high pH and that pH and Ω can decorrelate (Fig. 7) in situations with high photosynthesis and limited mixing of water masses.

4 Discussion

Temperate tidal pools are environments of extreme variability. In our pools, we observed seawater temperatures that could increase by up to 10 °C in a few hours compared to the adjacent ocean. During diurnal emersion periods, oxygen concentrations doubled, and pH could increase to pH 10 under present-day summer conditions. At night, pH routinely reached levels usually used as the "treatment" for ocean acidification perturbation experiments (∼ 7.6). Organisms present in the tidal pools may therefore already be adapted or acclimatized to extreme variability in pH and saturation state, which could affect their responses to ocean acidification (Andersson et al., 2015). For example, CCA from a site with naturally high pCO_2 variability calcified ∼ 50 % more than individuals from a nearby site of low variability when subjected to oscillating high pCO_2 treatments (Johnson et al., 2014). Here we show that, even in intertidal communities likely already acclimated or adapted to variable conditions, with potentially large phenotypic plasticity, acidification can still modify net community production and calcification rates.

4.1 Diurnal fertilization under CO_2 addition

Adding CO_2 to simulate future seawater acidification in the pools led to a diurnal fertilization effect. The community's net primary production increased by 20 % on average across all seasons, which was particularly visible in summer (+35 %), when temperatures/metabolic rates were high. Adding CO_2, we also added substrate for photosynthesis in the form of DIC (Fig. 3b) that the algae of the pools can assimilate, potentially supporting higher DIC use and algal primary production. This effect was apparent from the start of the emersion, suggesting a direct effect of increasing DIC concentration in the pools. It seems that photosynthesis in the pools was carbon-limited and that carbon addition therefore enhanced primary production in winter and to an even greater extent in summer. During photosynthesis, the uptake of inorganic carbon leads to a significant decrease in DIC – even under present-day conditions. Intertidal algae are typically adapted to this, with coralline algae in particular containing CCMs (CO₂ concentrating mechanisms) that allow them to achieve primary production in low DIC concentrations (Raven, 2011). Increasing seawater DIC may however promote an increase in active and/or passive CO_2 and HCO_3^- fluxes towards photosynthetic compartments. Borowitzka (1981) found that the photosynthetic rate of an intertidal CCA was highest at pH 6.5 to 7.5 (increased from pH 8.1), a change in pH that was achieved using HCl, suggesting that increased photosynthetic activity could also be linked to proton gradients/pumps and/or decreased energy expenditure
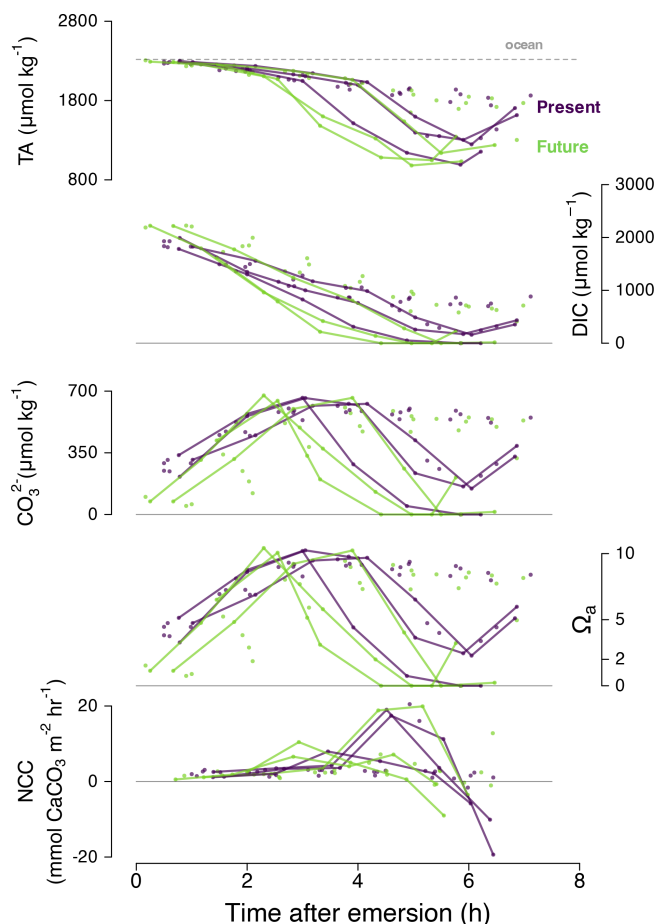
Figure 6. Time series for September 2020 diurnal data only: total alkalinity (TA; $\mu mol\,kg^{-1}$), dissolved inorganic carbon, CO_3^{2-} concentration ($\mu mol\,kg^{-1}$), aragonite saturation state (Ω_a) and NCC ($mmol\,m^{-2}\,h^{-1}$) with time after emersion by treatment (purple for present and green for future). The lines in bold represent individual Pools C and E, which switched from calcification to dissolution when pH_T was still above 9. A similar figure in the Supplement (Fig. S4) shows that sunset and irradiance are not correlated with the sudden change towards dissolution.

needed to operate CCMs rather than directly related to CO_2 gradients or higher substrate availability.

In winter and summer, pools under present-day and future conditions were autotrophic at emersion ($NCP_D > CR_N$; Fig. 5). If we consider the CPB to be integrated diurnal NCP and nocturnal CR over 24 h (assuming equal day–night duration), this means that the pools always fixed more carbon during the day than they respired at night at emersion ($NCP \gg CR$), regardless of treatment. One methodological uncertainty we highlight regarding net production is that diurnal DIC-derived NCP estimations were 50 % higher than O_2-derived NCP estimates ($NCP_{DIC} = 1.6 \pm 0.05\ NCP_{O_2}$ by day, $R^2 = 75$ %; Figs. 3c and 4). This discrepancy was far less apparent during nights, when methods agreed on respiration rates ($CR_{DIC} = 1.0 \pm 0.09\ CR_{O_2}$, $R^2 = 56$ %). While
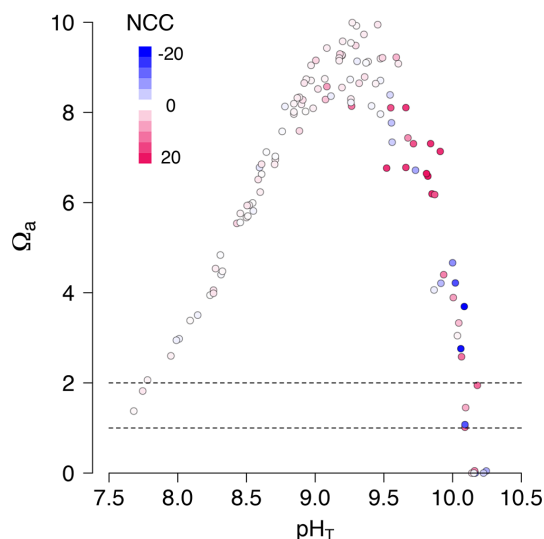

Figure 7. At very high pH there was both fast net calcification (red) and rapid net dissolution (blue). In some extreme cases, pH_T was not a good indicator of seawater saturation state (Ω_a). A selected dataset of diurnal low-tide emersion periods from September 2020. Colors represent NCC ($mmol\,CaCO_3\,m^{-2}\,h^{-1}$, as presented in Fig. 3c). Dashed horizontal lines represent saturation state for aragonite ($\Omega_a = 1$) and for high-Mg calcite ($\Omega_a = 2$).

O_2-derived NCP appears accurate during the night, O_2 production during the day is likely to have been underestimated due to degassing (e.g., visible formation of oxygen bubbles at the surface of algae, > 150 % air saturation by day vs. < 100 % at night). Thus, estimating diurnal net production using oxygen measurements may not be appropriate in algae-dominated environments such as these tidal pools. Nevertheless, despite the difference in absolute NCP estimates, both approaches indicate a diurnal fertilization effect.

4.2 Nocturnal dissolution under CO_2 addition

In the present study, natural mesocosms – temperate coralline-dominated tidal pools – were used to investigate the effect of ocean acidification on net calcification at the community level. As we observed a fertilization effect of CO_2 addition by day, we could have expected that it would also enhance diurnal calcification, as photosynthesis and calcification are tightly linked (Martin et al., 2013a, b; Williamson et al., 2017), but this was not observed. Treatment had no significant effect on the daytime net calcification rates, and diurnal variability in calcification appears to be predominately driven by PAR, temperature and metabolic activity (NCP). Increasing metabolic rates – in turn increasing calcification rates – however may have counterbalanced any calcification suppression or increased dissolution due to acidification, making its effect invisible. Noisette et al. (2013) similarly found no effect of pCO_2 treatment on light calcification for *E. elongata*. However, the authors reported a significant de-

crease in light calcification in *L. incrustans*; net calcification even switched to net dissolution in 750 and 1000 µatm pCO_2 treatments. While our future treatments started at pCO_2 levels higher than 1000 µatm, the fact that CO_2 addition did not influence diurnal calcification could also be due to favorable saturation state conditions in the micro-environment in which calcification occurs. The diffusive boundary layer (DBL) can enhance $CaCO_3$ precipitation micro-environment conditions due to the uptake of CO_2 OR DIC for photosynthesis. For instance, under light conditions, CCA surface pH has been shown to reach as high as 8.6 (Houlihan et al., 2020) in surrounding seawater at pH 7.7 (+1.1 pH units), which would be highly favorable to calcification. Although there are conflicting results indicating that saturation state of the ambient seawater is a key driver of coralline algal calcification, the biomineralization process in coralline algae has also been shown to present a certain degree of biological control (de Carvalho et al., 2017; Nash et al., 2019). Recent work using boron isotopes ($\delta 11B$) as a proxy for pH showed that coralline algae have the ability to elevate pH at their site of calcification (Cornwall et al., 2017). But more complex interactions may also be at work; e.g., CCA may use increases in HCO_3^- (due to CO_2 dissolution) to calcify, making them more resistant to ocean acidification, as suggested by Comeau et al. (2013).

There was net $CaCO_3$ dissolution in the pools at night (-0.7 mmol $CaCO_3$ m^{-2} h^{-1}), even when waters were still supersaturated with regard to aragonite under present-day conditions. Night dissolution may be a sign that the DBL of the calcifiers inhabiting the pools is undersaturated, possibly as a result of respiration. Indeed, Houlihan et al. (2020) observed that nocturnal algal respiration by CCA increased CO_2 in the DBL, decreasing pH of the DBL by 0.1 units. Such a small pH decrease alone is unlikely to explain an undersaturation of the calcifying environment as aragonite saturation state was still above 1.2 under most of the present-day conditions. However, given that the solubility of high-Mg calcite – the mineral composing *L. incrustans* and *E. elongata* in particular (Ries, 2011) – can be twice that of aragonite (Sulpis et al., 2021; Yamamoto et al., 2012), it is possible that undersaturation already occurs at night for this mineral even for $\Omega_a > 1$. Another reason for night dissolution might be linked to the patellid limpet, an opportunistic (Schaal and Grall, 2015) and dominant grazer in rock pools that can be particularly active at night (Lorenzen, 2007). Encrusting coralline algae can be an important food source for these herbivores, and the large percentage of grazed coralline algal $CaCO_3$ in their gut (Maneveldt et al., 2006) could dissolve easily at night.

Adding CO_2 (from 445 to 1500–2000 µatm) at the start of emersion significantly increased net dissolution (NCC_{lm}), by 40 % in summer and 70 % in winter. In a previous single-species experiment, Noisette et al. (2013) demonstrated that, for *L. incrustans* from an area close to our site, dark dissolution doubled with increasing pCO_2 (1000 µatm vs.

380 µatm), unlike *E. elongata*, for which there was no effect of pCO_2: the ACA even calcified in the dark up to 750 µatm (see also similar results from Egilsdottir et al., 2013). Since *L. incrustans* is the major calcifying species of the tidal pools we studied, it is likely that this species drives the results we observed at the pool community scale. Regardless of the treatment, nocturnal net dissolution rates (NCC) were also significantly correlated with Ω_a; the results are similar to those found by Kwiatkowski et al. (2016) in temperate tidal pools of California, without CO_2 addition.

In summer, pools under present-day and future conditions were precipitative (CCB > 0), meaning that diurnal net calcification exceeded nocturnal net dissolution, regardless of treatment. Adding CO_2 in summer did not consistently change CCB, with most pools showing little change in CCB due to treatment. By contrast, in the colder winter, the calcification budget was at least 50 % lower than in summer (present), with some pools having comparable net calcification during the day to net dissolution at night. During this season, adding CO_2 had variable impacts on CCB, decreasing it in three of the pools by more than 80 % and increasing relatively small CCB in two. These variable effects may be due to differences in community composition and highlight the difficulty in generalizing the results of natural mesocosm manipulations in which the initial community composition is not controlled. Nevertheless, we expected CO_2 addition to have a greater negative effect in winter (more dissolution) than in summer, with saturation states being lower due to colder temperatures, making it more of a "crucial"/"bottleneck" season. This emphasizes the need to study the effect of ocean acidification across seasons and temperature ranges, especially given the associated changes in algal community composition and metabolic activity.

A limit of the CCB in the current study is that we only considered the tidal pools to be closed (emersed) systems. However, in an acidifying ocean, tidal pool communities are submersed for nearly 12 h d^{-1}, resulting in long exposure to low pH. More accurate and realistic budgets would need to integrate these immersion periods, which might have additive negative effects on calcification (see, e.g., Legrand et al., 2018b, for tidal assemblage experiments on net production/respiration).

4.3 Instances of aragonite undersaturation at high pH

An unexpected phenomenon happened in Pools C and E in summer: although we measured very high pH values, we observed that total alkalinity suddenly increased, a sign of fast net dissolution. When we then computed the carbonate chemistry, the saturation states were surprisingly low ($\Omega_a = 0$ for $pH_T = 10$), which was due to near-zero DIC concentrations – and thus near-zero CO_3^{2-} concentrations. Under these particular conditions, which occurred towards the end of the tidal emersion period, any $CaCO_3$ precipitation was less than dissolution; precipitation may even have

been impossible due to a lack of DIC substrate. In intertidal pools with a high density of *Zostera marina*, Miller and Kelley (2021) observed a similar decoupling between pH and Ω_a, with increases in pH not leading to an increase in saturation state at high pH values due to a lack of DIC OR CO_3^{2-}. In our study, we observed even more drastic decoupling between expected changes in pH, Ω_a and NCC, with some of the fastest net dissolution rates observed at very high pH and very low Ω_a values that were a consequence of near-complete consumption of DIC by community production (Fig. 7). Macroalgae cultivation has been proposed as a method of bioremediation for local acidification, in particular to improve aquaculture environments (e.g., Bergstrom et al., 2019; Gao and Beardall, 2022): an increase in algal or marine plant cover would reverse or buffer the negative effects of acidification on heterotroph calcifiers. Our results and those of Miller and Kelley (2021) suggest that phytoremediation should not consider pH to be the sole indicator for "acidification remediation" and that periodical decreases in saturation state in macroalgae- or seaweed-dominated environments in summer (and during marine heat waves) may need to be considered for these proposed types of remediations.

5 Conclusion

Relative to its area, human societies are disproportionately reliant on the coastal ocean for the provision of natural resources and climate regulation. Yet our understanding of how anthropogenic carbon emissions and associated ocean acidification will influence natural coastal ecosystems and community metabolism remains limited. In the present study, we manipulated the carbonate chemistry of natural temperate intertidal pools to explore the potential impact of future ocean acidification on community-level calcification and production. We find evidence of large seasonal, diel and community-specific differences in the sensitivity of intertidal community metabolism to acidification. Diurnally, acidification was found to enhance net community production, with this fertilization effect indicating that algal photosynthesis is naturally carbon-limited in such environments at emersion. Diurnal net community calcification was unaffected by acidification. In contrast, nocturnal acidification resulted in greater net community dissolution in the intertidal pools yet had no consistent effect on community respiration. Integrated over day/night emersion periods, the intertidal mesocosms maintained positive net community calcification and production under both present-day and future conditions. Despite considerable differences between individual pools and strong seasonal dependencies, our results indicate that the net calcification and production of temperate intertidal communities – likely acclimated/adapted to variable conditions – could be affected by future acidification.

References

Albright, R., Caldeira, L., Hosfelt, J., Kwiatkowski, L., Maclaren, J. K., Mason, B. M., Nebuchina, Y., Ninokawa, A., Pongratz, J., Ricke, K. L., Rivlin, T., Schneider, K., Sesboüé, M., Shamberger, K., Silverman, J., Wolfe, K., Zhu, K., and Caldeira, K.: Reversal of ocean acidification enhances net coral reef calcification, Nature, 531, 362–365, https://doi.org/10.1038/nature17155, 2016.

Albright, R., Takeshita, Y., Koweek, D. A., Ninokawa, A., Wolfe, K., Rivlin, T., Nebuchina, Y., Young, J., and Caldeira, K.: Carbon dioxide addition to coral reef waters suppresses net community calcification, Nature, 555, 516–519, https://doi.org/10.1038/nature25968, 2018.

Aminot, A. and Kérouel, R.: Dosage automatique des nutriments dans les eaux marines: méthodes en flux continu, Editions Quae, 191 pp., ISBN 978-2-7592-0023-8, 2007.

Andersson, A. J., Kline, D. I., Edmunds, P. J., Archer, S. D., Bednaršek, N., Carpenter, R. C., Chadsey, M., Goldstein, P., Grottoli, A. G., Hurst, T. P., King, A. L., Kübler, J. E., Kuffner, I. B., Mackey, K. R. M., Menge, B. A., Paytan, A., Riebesell, U., Schnetzer, A., Warner, M. E., and Zimmerman, R. C.: Understanding ocean acidification impacts on organismal to ecological scales, Oceanography, 28, 16–27, 2015.

Barry, J., Hall-Spencer, J., and Tyrrell, T.: In situ perturbation experiments: natural venting sites, spatial/temporal gradients in ocean pH, manipulative in situ $p\mathrm{CO_2}$ perturbations, in: Guide to best practices in ocean acidification research and data reporting, , edited by: Riebesell, U., Fabry, V. J., Hansson, L., and Gattuso, J.-P., Publications Office of the European Union, Luxembourg, 123–136, https://doi.org/10.2777/66906, 2010.

Bergstrom, E., Silva, J., Martins, C., and Horta, P.: Seagrass can mitigate negative ocean acidification effects on calcifying algae, Sci. Rep., 9, 1932, https://doi.org/10.1038/s41598-018-35670-3, 2019.

Borowitzka, M. A.: Photosynthesis and calcification in the articulated coralline red algae *Amphiroa anceps* and *A. foliacea*, Mar. Biol., 62, 17–23, https://doi.org/10.1007/BF00396947, 1981.

Bracken, M. E. S., Miller, L. P., Mastroni, S. E., Lira, S. M., and Sorte, C. J. B.: Accounting for variation in temperature and oxygen availability when quantifying marine ecosystem metabolism, Sci. Rep., 12, 825, https://doi.org/10.1038/s41598-021-04685-8, 2022.

Cocquempot, L., Delacourt, C., Paillet, J., Riou, P., Aucan, J., Castelle, B., Charria, G., Claudet, J., Conan, P., Coppola, L., Hocdé, R., Planes, S., Raimbault, P., Savoye, N., Testut, L., and Vuillemin, R.: Coastal ocean and nearshore observation: a French case study, Front. Mar. Sci., 6, 324, https://doi.org/10.3389/fmars.2019.00324, 2019.

Comeau, S., Carpenter, R. C., and Edmunds, P. J.: Coral reef calcifiers buffer their response to ocean acidification using both bicarbonate and carbonate, P. R. Soc. B-Biol. Sci., 280, 20122374, https://doi.org/10.1098/rspb.2012.2374, 2013.

Cornwall, C. E., Comeau, S., and McCulloch, M. T.: Coralline algae elevate pH at the site of calcification under ocean acidification, Glob. Change Biol., 23, 4245–4256, https://doi.org/10.1111/gcb.13673, 2017.

Cox, T. E., Schenone, S., Delille, J., Díaz-Castañeda, V., Alliouane, S., Gattuso, J.-P., and Gazeau, F.: Effects of ocean acidification on *Posidonia oceanica* epiphytic community and shoot productivity, J. Ecol., 103, 1594–1609, https://doi.org/10.1111/1365-2745.12477, 2015.

de Carvalho, R. T., Salgado, L. T., Amado Filho, G. M., Leal, R. N., Werckmann, J., Rossi, A. L., Campos, A. P. C., Karez, C. S., and Farina, M.: Biomineralization of calcium carbonate in the cell wall of Lithothamnion crispatum (Hapalidiales, Rhodophyta): correlation between the organic matrix and the mineral phase, J. Phycol., 53, 642–651, https://doi.org/10.1111/jpy.12526, 2017.

Dickson, A., Sabine, C. L., and Christian, J. R.: Guide to best practices for ocean $\mathrm{CO_2}$ measurements, PICES Special Publication 3, 191 pp., ISBN 1-897176-07-4, 2007.

Dorey, N., Lançon, P., Thorndyke, M., and Dupont, S.: Assessing physiological tipping point of sea urchin larvae exposed

to a broad range of pH, Glob. Change Biol., 19, 3355–3367, https://doi.org/10.1111/gcb.12276, 2013.

Egilsdottir, H., Noisette, F., Noël, L. M.-L. J., Olafsson, J., and Martin, S.: Effects of $p\mathrm{CO_2}$ on physiology and skeletal mineralogy in a tidal pool coralline alga *Corallina elongata*, Mar. Biol., 160, 2103–2112, https://doi.org/10.1007/s00227-012-2090-7, 2013.

Foo, S., Byrne, M., Ricevuto, E., and Gambi, M. C.: The carbon dioxide vents of Ischia, Italy, a natural system to assess impacts of ocean acidification on marine ecosystems: An overview of research and comparisons with other vent systems, Oceanogr. Mar. Biol., 56, 237–310, https://doi.org/10.1201/9780429454455-4, 2018.

Ganning, B.: Studies on chemical, physical and biological conditions in swedish rockpool ecosystems, Ophelia, 9, 51–105, https://doi.org/10.1080/00785326.1971.10430090, 1971.

Gao, K. and Beardall, J.: Using macroalgae to address UN Sustainable Development goals through $\mathrm{CO_2}$ remediation and improvement of the aquaculture environment, Appl. Phycol., 3, 360–367, https://doi.org/10.1080/26388081.2022.2025617, 2022.

Gattuso, J.-P., Epitalon, J.-M., Lavigne, H., and Orr, J.: seacarb: seawater carbonate chemistry with R, R package version 3.2.16, http://CRAN.R-project.org/package=seacarb (last access: 1 June 2021), 2021.

Gazeau, F., Urbini, L., Cox, T., Alliouane, S., and Gattuso, J.: Comparison of the alkalinity and calcium anomaly techniques to estimate rates of net calcification, Mar. Ecol. Prog. Ser., 527, 1–12, https://doi.org/10.3354/meps11287, 2015.

Gran, G.: Determination of the equivalence point in potentiometric titrations. Part II, The Analyst, 77, 661, https://doi.org/10.1039/an9527700661, 1952.

Haraldsson, C., Anderson, L. G., Hassellöv, M., Hulth, S., and Olsson, K.: Rapid, high-precision potentiometric titration of alkalinity in ocean and sediment pore waters, Deep-Sea Res. Part Oceanogr. Res.-Pt. I, 44, 2031–2044, https://doi.org/10.1016/S0967-0637(97)00088-5, 1997.

Houlihan, E. P., Espinel-Velasco, N., Cornwall, C. E., Pilditch, C. A., and Lamare, M. D.: Diffusive boundary layers and ocean acidification: Implications for sea urchin settlement and growth, Front. Mar. Sci., 7, 577562, https://doi.org/10.3389/fmars.2020.577562, 2020.

Hurd, C. L., Beardall, J., Comeau, S., Cornwall, C. E., Havenhand, J. N., Munday, P. L., Parker, L. M., Raven, J. A., McGraw, C. M., Hurd, C. L., Beardall, J., Comeau, S., Cornwall, C. E., Havenhand, J. N., Munday, P. L., Parker, L. M., Raven, J. A., and McGraw, C. M.: Ocean acidification as a multiple driver: how interactions between changing seawater carbonate parameters affect marine life, Mar. Freshwater Res., 71, 263–274, https://doi.org/10.1071/MF19267, 2019.

IPCC: IPCC Special Report on the Ocean and Cryosphere in a Changing Climate, edited by: Pörtner, H. O., Roberts, D., Masson-Delmotte, V., and Zhai, P., Cambridge University Press, UK, 755 pp., https://doi.org/10.1017/9781009157964, 2019.

Jia, G., E. Shevliakova, P. Artaxo, N. De Noblet-Ducoudré, R. Houghton, J. House, K. Kitajima, C. Lennard, A. Popp, A. Sirin, R. Sukumar, and L. Verchot: Land–climate interactions., in: Climate Change and Land: an IPCC special report on climate change, desertification, land degradation, sustainable land management, food security, and greenhouse gas fluxes in terrestrial ecosystems, https://doi.org/10.1017/9781009157988.001, 2019.

Johnson, M. D., Moriarty, V. W., and Carpenter, R. C.: Acclimatization of the Crustose Coralline Alga Porolithon onkodes to Variable pCO_2, PLOS ONE, 9, e87678, https://doi.org/10.1371/journal.pone.0087678, 2014.

Kottmeier, D. M., Chrachri, A., Langer, G., Helliwell, K. E., Wheeler, G. L., and Brownlee, C.: Reduced H+ channel activity disrupts pH homeostasis and calcification in coccolithophores at low ocean pH, P. Natl. Acad. Sci. USA, 119, e2118009119, https://doi.org/10.1073/pnas.2118009119, 2022.

Kroeker, K. J., Micheli, F., and Gambi, M. C.: Ocean acidification causes ecosystem shifts via altered competitive interactions, Nat. Clim. Change, 3, 156–159, https://doi.org/10.1038/nclimate1680, 2013.

Kwiatkowski, L., Gaylord, B., Hill, T., Hosfelt, J., Kroeker, K. J., Nebuchina, Y., Ninokawa, A., Russell, A. D., Rivest, E. B., Sesboüé, M., and Caldeira, K.: Nighttime dissolution in a temperate coastal ocean ecosystem increases under acidification, Sci. Rep., 6, 22984, https://doi.org/10.1038/srep22984, 2016.

Kwiatkowski, L., Torres, O., Bopp, L., Aumont, O., Chamberlain, M., Christian, J. R., Dunne, J. P., Gehlen, M., Ilyina, T., John, J. G., Lenton, A., Li, H., Lovenduski, N. S., Orr, J. C., Palmieri, J., Santana-Falcón, Y., Schwinger, J., Séférian, R., Stock, C. A., Tagliabue, A., Takano, Y., Tjiputra, J., Toyama, K., Tsujino, H., Watanabe, M., Yamamoto, A., Yool, A., and Ziehn, T.: Twenty-first century ocean warming, acidification, deoxygenation, and upper-ocean nutrient and primary production decline from CMIP6 model projections, Biogeosciences, 17, 3439–3470, https://doi.org/10.5194/bg-17-3439-2020, 2020.

Legrand, E., Riera, P., Pouliquen, L., Bohner, O., Cariou, T., and Martin, S.: Ecological characterization of intertidal rockpools: Seasonal and diurnal monitoring of physico-chemical parameters, Reg. Stud. Mar. Sci., 17, 1–10, https://doi.org/10.1016/j.rsma.2017.11.003, 2018a.

Legrand, E., Riera, P., Bohner, O., Coudret, J., Schlicklin, F., Derrien, M., and Martin, S.: Impact of ocean acidification and warming on the productivity of a rock pool community, Mar. Environ. Res., 136, 78–88, https://doi.org/10.1016/j.marenvres.2018.02.010, 2018b.

Legrand, E., Riera, P., Lutier, M., Coudret, J., Grall, J., and Martin, S.: Grazers increase the sensitivity of coralline algae to ocean acidification and warming, J. Sea Res., 148–149, 1–7, https://doi.org/10.1016/j.seares.2019.03.001, 2019.

Lorenzen, S.: The limpet *Patella vulgata* L. at night in air: effective feeding on *Ascophyllum nodosum* monocultures and stranded seaweeds, J. Mollus. Stud., 73, 267–274, https://doi.org/10.1093/mollus/eym022, 2007.

Mackey, K. R. M., Morris, J. J., Morel, F. M. M., and Kranz, S. A.: Response of photosynthesis to ocean acidification, Oceanography, 28, 74–91, 2015.

Maneveldt, G. W., Wilby, D., Potgieter, M., and Hendricks, M. G. J.: The role of encrusting coralline algae in the diets of selected intertidal herbivores, J. Appl. Phycol., 18, 619–627, https://doi.org/10.1007/s10811-006-9059-1, 2006.

Martin, S., Cohu, S., Vignot, C., Zimmerman, G., and Gattuso, J.-P.: One-year experiment on the physiological response of the Mediterranean crustose coralline alga, *Lithophyllum cabiochae*, to elevated pCO_2 and temperature, Ecol. Evol., 3, 676–693, https://doi.org/10.1002/ece3.475, 2013a.

Martin, S., Charnoz, A., and Gattuso, J.-P.: Photosynthesis, respiration and calcification in the Mediterranean crustose coralline alga *Lithophyllum cabiochae* (Corallinales, Rhodophyta), Eur. J. Phycol., 48, 163–172, https://doi.org/10.1080/09670262.2013.786790, 2013b.

Miller, C. A. and Kelley, A. L.: Alkalinity cycling and carbonate chemistry decoupling in seagrass mystify processes of acidification mitigation, Sci. Rep., 11, 13500, https://doi.org/10.1038/s41598-021-92771-2, 2021.

Morris, S. and Taylor, A. C.: Diurnal and seasonal variation in physico-chemical conditions within intertidal rock pools, Estuar. Coast. Shelf S., 17, 339–355, https://doi.org/10.1016/0272-7714(83)90026-4, 1983.

Nash, M. C., Diaz-Pulido, G., Harvey, A. S., and Adey, W.: Coralline algal calcification: A morphological and process-based understanding, PLOS ONE, 14, e0221396, https://doi.org/10.1371/journal.pone.0221396, 2019.

Noisette, F., Egilsdottir, H., Davoult, D., and Martin, S.: Physiological responses of three temperate coralline algae from contrasting habitats to near-future ocean acidification, J. Exp. Mar. Biol. Ecol., 448, 179–187, https://doi.org/10.1016/j.jembe.2013.07.006, 2013.

Paiva, F., Brennecke, D., Pansch, C., and Briski, E.: Consistency of aquatic enclosed experiments: The importance of scale and ecological complexity, Divers. Distrib., 27, 524–532, 2021.

Pan, T.-C. F., Applebaum, S. L., and Manahan, D. T.: Experimental ocean acidification alters the allocation of metabolic energy, P. Natl. Acad. Sci. USA, 112, 4696–701, https://doi.org/10.1073/pnas.1416967112, 2015.

Pansch, A., Winde, V., Asmus, R., and Asmus, H.: Tidal benthic mesocosms simulating future climate change scenarios in the field of marine ecology, Limnol. Oceanogr.-Meth., 14, 257–267, https://doi.org/10.1002/lom3.10086, 2016.

Pinheiro, J., Bates, D., and R-core: Package "nlme": Linear and Nonlinear Mixed Effects Models, Cran-R, https://CRAN.R-project.org/package=nlme (last access: 1 June 2019), 2018.

Raven, J. A.: Effects on marine algae of changed seawater chemistry with increasing atmospheric CO_2, Biol. Environ., 111, 1–17, 2011.

R Core Team: R: A language and environment for statistical computing, R Foundation for Statistical Computing, Vienna, Austria, https://www.R-project.org/ (last access: 1 June 2017), 2017.

Riebesell, U., Czerny, J., von Bröckel, K., Boxhammer, T., Büdenbender, J., Deckelnick, M., Fischer, M., Hoffmann, D., Krug, S. A., Lentz, U., Ludwig, A., Muche, R., and Schulz, K. G.: Technical Note: A mobile sea-going mesocosm system – new opportunities for ocean change research, Biogeosciences, 10, 1835–1847, https://doi.org/10.5194/bg-10-1835-2013, 2013.

Ries, J. B.: Skeletal mineralogy in a high-CO_2 world, J. Exp. Mar. Biol. Ecol., 403, 54–64, https://doi.org/10.1016/j.jembe.2011.04.006, 2011.

Ries, J. B., Ghazaleh, M. N., Connolly, B., Westfield, I., and Castillo, K. D.: Impacts of seawater saturation state (Ω A = 0.4–4.6) and temperature (10, 25 °C) on the dissolution kinetics of whole-shell biogenic carbonates, Geochim. Cosmochim. Ac., 192, 318–337, https://doi.org/10.1016/j.gca.2016.07.001, 2016.

Schaal, G. and Grall, J.: Microscale aspects in the diet of the limpet Patella vulgata L., J. Mar. Biol. Assoc. UK, 95, 1155–1162, https://doi.org/10.1017/S0025315415000429, 2015.

Schulz, K. G., Bellerby, R. G. J., Brussaard, C. P. D., Büdenbender, J., Czerny, J., Engel, A., Fischer, M., Koch-Klavsen, S., Krug, S. A., Lischka, S., Ludwig, A., Meyerhöfer, M., Nondal, G., Silyakova, A., Stuhr, A., and Riebesell, U.: Temporal biomass dynamics of an Arctic plankton bloom in response to increasing levels of atmospheric carbon dioxide, Biogeosciences, 10, 161–180, https://doi.org/10.5194/bg-10-161-2013, 2013.

Smith, S. V. and Key, G. S.: Carbon dioxide and metabolism in marine environments, Limnol. Oceanogr., 20, 493–495, https://doi.org/10.4319/lo.1975.20.3.0493, 1975.

Spisla, C., Taucher, J., Bach, L. T., Haunost, M., Boxhammer, T., King, A. L., Jenkins, B. D., Wallace, J. R., Ludwig, A., Meyer, J., Stange, P., Minutolo, F., Lohbeck, K. T., Nauendorf, A., Kalter, V., Lischka, S., Sswat, M., Dörner, I., Ismar-Rebitz, S. M. H., Aberle, N., Yong, J. C., Bouquet, J.-M., Lechtenbörger, A. K., Kohnert, P., Krudewig, M., and Riebesell, U.: Extreme levels of ocean acidification restructure the plankton community and biogeochemistry of a temperate coastal ecosystem: A mesocosm study, Front. Mar. Sci., 7, 611157, https://doi.org/10.3389/fmars.2020.611157, 2021.

Stumpp, M., Hu, M. Y., Casties, I., Saborowski, R., Bleich, M., Melzner, F., and Dupont, S.: Digestion in sea urchin larvae impaired under ocean acidification, Nat. Clim. Change, 3, 1044–1049, https://doi.org/10.1038/nclimate2028, 2013.

Sulpis, O., Lauvset, S. K., and Hagens, M.: Current estimates of K_1^* and K_2^* appear inconsistent with measured CO_2 system parameters in cold oceanic regions, Ocean Sci., 16, 847–862, https://doi.org/10.5194/os-16-847-2020, 2020.

Sulpis, O., Jeansson, E., Dinauer, A., Lauvset, S. K., and Middelburg, J. J.: Calcium carbonate dissolution patterns in the ocean, Nat. Geosci., 14, 423–428, https://doi.org/10.1038/s41561-021-00743-y, 2021.

Torres, O., Kwiatkowski, L., Sutton, A. J., Dorey, N., and Orr, J. C.: Characterizing mean and extreme diurnal variability of ocean CO_2 system variables across marine environments, Geophys. Res. Lett., 48, e2020GL090228, https://doi.org/10.1029/2020GL090228, 2021.

Widdicombe, S., Dupont, S., and Thorndyke, M.: Laboratory experiments and benthic mesocosm studies, in: Guide to best practices for ocean acidification research and data reporting, edited by: Riebesell, U., Fabry, V. J., Hansson, L., and Gattuso, J.-P., Publications Office of the European Union, Luxembourg, https://doi.org/10.2777/66906, 2010.

Williamson, C. J., Perkins, R., Voller, M., Yallop, M. L., and Brodie, J.: The regulation of coralline algal physiology, an in situ study of Corallina officinalis (*Corallinales, Rhodophyta*), Biogeosciences, 14, 4485–4498, https://doi.org/10.5194/bg-14-4485-2017, 2017.

Yamamoto, S., Kayanne, H., Terai, M., Watanabe, A., Kato, K., Negishi, A., and Nozaki, K.: Threshold of carbonate saturation state determined by CO_2 control experiment, Biogeosciences, 9, 1441–1450, https://doi.org/10.5194/bg-9-1441-2012, 2012.